ACS Energy LETTERS

http://pubs.acs.org/journal/aelccp

LETTER

Tailored Cathode Composite Microstructure Enables Long Cycle Life at Low Pressure for All-Solid-State Batteries

Ke Zhou, Sijian Lu, Charles Mish, Yu-Ting Chen, Shijie Feng, Jiyoung Kim, Min-Sang Song, Hyunsun Alicia Kim,* and Ping Liu*

Cite This: *ACS Energy Lett.* 2025, 10, 966−974

Read Online

ACCESS | Metrics & More | Article Recommendations | Supporting Information

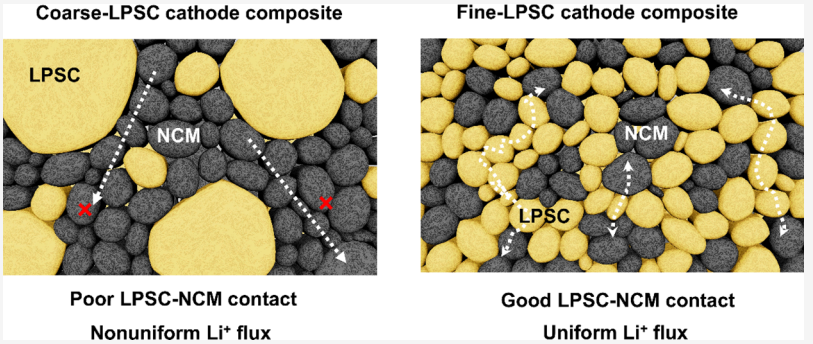

ABSTRACT: **The practical application of all-solid-state batteries (ASSBs) requires reliable operation at low pressures, which remains a significant challenge. In this work, we examine the role of a cathode composite microstructure composed of solid-state electrolyte (SSE) with different particle sizes. A composite made of $LiNi_{0.8}Co_{0.1}Mn_{0.1}O_2$ (NCM811) and fine-particle Li_6PS_5Cl (LPSC) shows a more uniform distribution of SSE on the surface of NCM811 particles, ensuring intimate contact. Moreover, the composite features reduced tortuosity, which enhances Li ion conduction. These microstructural advantages result in significantly reduced charge transfer resistance, helping to suppress mechanical distortion and electrochemical degradation during cycling under low-pressure conditions. As a result, the fine-LPSC cathode composite exhibits enhanced cycling stability at a moderate stack pressure of 2 MPa, outperforming its coarse-LPSC counterpart. Our finding confirms the important role of microstructure design in enabling high-performance ASSBs operating under low-pressure conditions.**

Downloaded via UNIV OF CALIFORNIA SAN DIEGO on January 25, 2025 at 20:32:23 (UTC).
See https://pubs.acs.org/sharingguidelines for options on how to legitimately share published articles.

All-solid-state lithium batteries (ASSBs) utilizing non-flammable solid-state electrolytes (SSEs), coupled with layered oxide cathodes and lithium metal anodes, have garnered significant attention for their potential to achieve higher energy densities and improved safety in next-generation energy storage systems.[1,2] However, ASSBs face several challenges compared to conventional liquid electrolyte batteries, including insufficient capacity, low Coulombic efficiency, low power density, and rapid capacity degradation.[3,4] An important cause of these issues lies in the composition of the cathode electrode, which consists of cathode active materials (CAMs) directly surrounded by SSE particles.[5] This configuration introduces several limitations: (1) incomplete physical contact between all solid particles (solid−solid contact), (2) the inability of SSE to infiltrate the gaps and voids between particles, (3) volume changes in CAM during (de)lithiation that disrupt architectural stability due to lattice expansion and distortion, and (4) delamination at the CAM-SSE interface.[6−9] These factors prevent the formation of a homogeneous ion percolation network, hindering lithium-ion conduction within the cathode composite and compromising electrochemical performance.[9,10]

These challenges necessitate the use of high stack pressures to ensure adequate contact between the cathode and SSE.[11] For example, Sakka et al. employed X-ray computed tomography (CT) to investigate the effect of stack pressure

Received: November 24, 2024
Revised: December 30, 2024
Accepted: January 22, 2025

© XXXX American Chemical Society

https://doi.org/10.1021/acsenergylett.4c03256
ACS Energy Lett. 2025, 10, 966−974

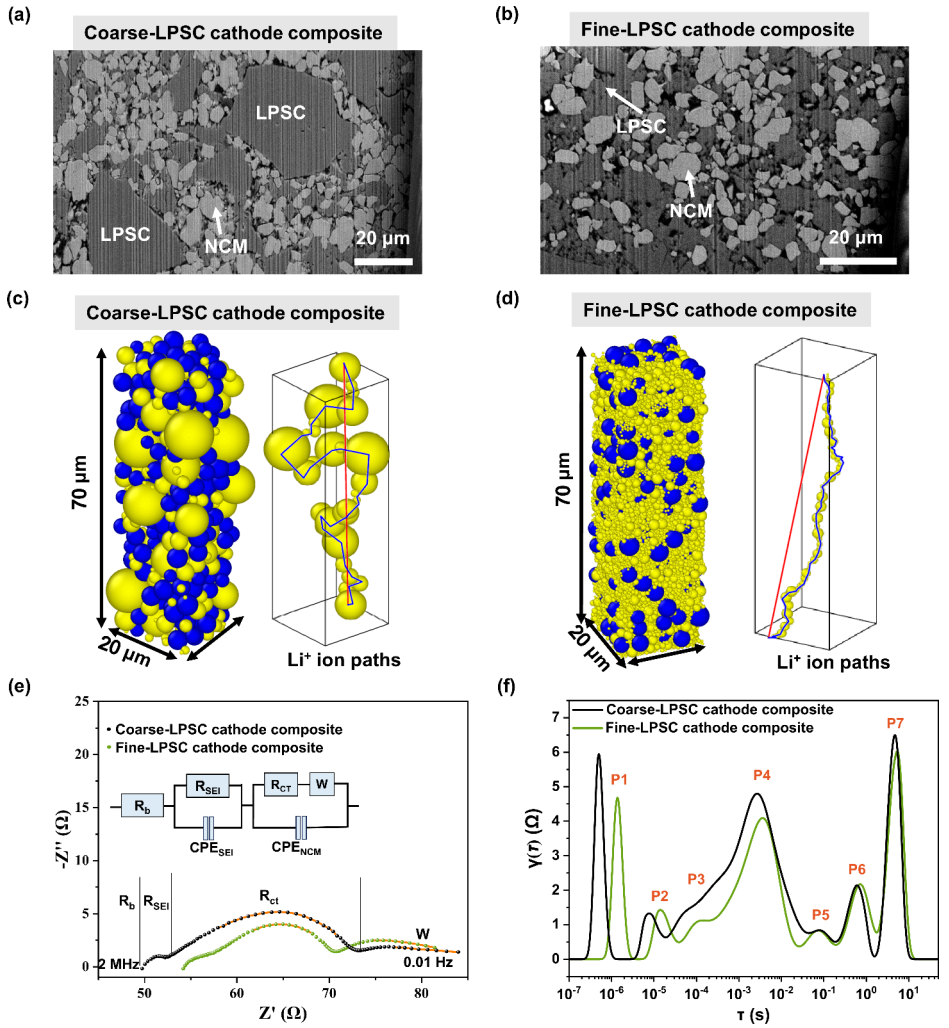

Figure 1. Characterizations of the cathode composites. FIB-SEM cross-sectional images for the coarse-LPSC cathode composite (a) and the fine-LPSC cathode composite (b). Schematic diagram of the cathode composite and Li^+ ion tortuosity for the coarse-LPSC cathode composite (c) and the fine-LPSC cathode composite (d). (e) Nyquist plots of the coarse-LPSC and fine-LPSC cathode composites, along with the equivalent circuit model. (f) Corresponding DRT plots for both cathode composites.

on the CAM-SSE interface. They found that at high pressures (50 MPa), SSE particles filled internal cavities within the cathode composite, significantly improving the contact area fraction compared to conditions at or below 12 MPa, resulting in a notable reduction in charge transfer resistance.[12] A model developed to assess the stability of the CAM-SSE contact showed that a pressure of 25 MPa was sufficient to maintain a stable interfacial contact. However, the requirement for such high pressures increases production costs and reduces the overall energy density at the pack level. To achieve high-energy-density ASSBs, industry generally aims to operate at or below 5 MPa. Therefore, there is a clear need for improved processing techniques to reduce reliance on such high pressures.

From the above discussion, it is clear that a key strategy for enhancing the performance of ASSBs under low pressure is to design a cathode composite microstructure that ensures optimal interfacial contact between the CAM and SSE. Studies have shown that smaller SSE particles (around 4 μm) enhance charge transport properties.[13] Tan et al. showed through both modeling and experiments that reducing the size of SSE particles can improve cathode utilization.[14] Likewise, reducing the size of CAM particles can also offer more contact points between CAM and SSE, leading to improved performance.[15] A hierarchical composite structure that combines small (~300 nm to 4 μm) and large (~20 μm) $Li_{5.5}PS_{4.5}Cl_{1.5}$ particles with CAM was shown to result in a lower tortuosity and faster lithium (Li) ion transport.[16] Research has shown that coating an SSE layer onto the surface of CAM particles can establish intimate interfacial contact, leading to improved performance even at low pressures.[17−19] Thus, improved design of a cathode composite microstructure holds great promise for developing ASSBs with higher energy densities, lower stack pressures, and stable long-term performance. An ideal microstructure should feature intimate contact between the SSE and CAM while maintaining robust SSE pathways with low tortuosity to facilitate Li ion transport.

In this study, we report a wet roll-mixing method to produce fine-LPSC powder, which facilitates the preparation of a high-performance fine-LPSC cathode composite architecture with enhanced cathode utilization and low tortuosity. Our approach results in a more uniform distribution of LPSC around the $LiNi_{0.8}Co_{0.1}Mn_{0.1}O_2$ (NCM811) particles (~1 to 5 μm) within the composite, ensuring a larger, more intimate interfacial contact and establishing an efficient Li ion percolation network. This microstructural improvement leads to higher

https://doi.org/10.1021/acsenergylett.4c03256
ACS Energy Lett. 2025, 10, 966−974

capacity, improved long-term cycle stability, and better rate performance, all of which are achievable at low pressure. More importantly, our work underscores the critical role of the cathode composite microstructure in optimizing electrochemical performance at low pressures, offering valuable insights for industrial-scale ASSB development.

Various synthesis methods were employed to produce fine-LPSC powders (Figure S1), including ball-milling without solvent (denoted as LPSC ball-milling), roll-milling without solvent (LPSC rolling), ball-milling with toluene solution (LPSC@To ball-milling), and roll-milling with toluene solution (LPSC@To rolling).[20] As shown in Figure S2, the particle sizes of all synthesized fine-LPSC powders decrease (~1 μm) with these methods. In addition, the particles prepared by the ball-milling process are smaller than those that were roll-milled (Figure S3). This is to be expected due to the high energy involved in the ball-milling process. When comparing the fine-LPSC prepared in the presence of toluene, the roll milled material has much less fraction of very small particles of <0.25 μm while preserving an appreciable number of particles of >3 μm in size. This particle size distribution is advantageous in generating a uniform cathode composite structure with low tortuosity.[16] Moreover, the X-ray diffraction (XRD) pattern of LPSC ball-milling reveals the presence of Li_2S impurities (Figure S4). In contrast, the XRD pattern of LPSC@To rolling is similar to that of coarse-LPSC. Additionally, electrochemical impedance spectroscopy (EIS) results (Figure S5) show that the ionic conductivity of the LPSC@To rolling electrolyte is the highest among the fine-LPSC samples, indicating that the roll-mixing process with toluene minimizes adverse effects on the LPSC and preserves its original properties.

Next, we provide a detailed comparison between coarse-LPSC and fine-LPSC prepared using the LPSC@To rolling electrolyte. The residual toluene content was measured via thermogravimetric analysis (TGA). The decomposition temperature for both electrolytes is approximately 365 °C (Figure S6), with no new peaks observed, indicating that the fine-LPSC contains no residual toluene solution. Figure S7 presents the pore size distribution profiles of both electrolyte pellets obtained through focused ion beam (FIB) cross-sectional scanning electron microscopy (SEM). The coarse-LPSC pellet exhibits 11.3% surface porosity, while the fine-LPSC pellet shows only 4.4% porosity, indicating a denser structure. Additionally, the relative density of fine-LPSC is 90% (Figure S8), demonstrating that the fine-LPSC powders achieve a significantly higher relative density. The specific surface area of the electrolytes was assessed by using the Brunauer–Emmett–Teller (BET) method (Figure S9). The coarse-LPSC and fine-LPSC exhibit surface areas of 6.02 and 9.24 m^2/g, respectively, showing that the roll-mixing process increases the surface area, in agreement with the SEM observations. Therefore, fine-LPSC is expected to show improved interfacial contact between the CAM and LPSC, contributing to enhanced performance.

To examine the distribution of LPSC around the CAM of NCM811, we analyzed the FIB cross-sectional SEM images of both coarse-LPSC and fine-LPSC cathode composites (Figures S10 and S11). Multiple images are shown to illustrate the uniformity of the microstructure. Energy-dispersive X-ray (EDX) mapping of the Ni and P signals was used to characterize NCM811 (small particles) and LPSC (large particles), respectively. The results show that the coarse-LPSC cathode composite exhibits significant agglomeration of LPSC particles, with a heterogeneous distribution of LPSC around the NCM811 particles (Figures 1a and S12). In contrast, the fine-LPSC cathode composite shows a more uniform distribution of LPSC particles around NCM811, resulting in a more homogeneous microstructure (Figures 1b and S13).

Moreover, we investigated the cathode utilization and Li ion transport tortuosity for both cathode composites modeled using discrete spherical particles (Figure S14). The interparticle forces were simulated using Hertzian contact within the granular package of LAMMPS software.[21] To model the calendaring process, we employed velocity-Verlet time integration with explicit time steps in the microsecond range, ensuring numerical stability. CAM utilization was calculated by measuring the percentage of NCM811 particles in contact with LPSC particles.[14] A table summarizing the CAM utilization for different contact criteria (defined by the minimum overlap between two particles relative to the sum of their radii) is provided in Table 1. The simulations predict that the coarse-LPSC cathode composite would exhibit a lower CAM utilization. For example, at a 2% overlap, the fine-LPSC cathode composite achieves nearly 100% CAM utilization, significantly higher than the 83% utilization observed in the coarse-LPSC cathode composite (with unused red atoms shown in Figure S14e). This indicates that the fine-LPSC cathode composite can deliver higher capacity due to its superior interparticle contact.

Table 1. Summary of the CAM utilization

Configuration	Minimum Overlap	CAM Utilization
Coarse-LPSC	0%	94%
	2%	83%
	5%	56%
	10%	20%
Fine-LPSC	0%	100%
	2%	100%
	5%	94%
	10%	28%

The tortuosity of the LPSC pathways, a crucial factor in determining effective ionic conductivity in batteries, was analyzed for both cathode composites (Figure S15).[22] Quantitatively, the fine-LPSC cathode composite exhibits a median tortuosity of 1.21, compared to 1.84 for the coarse-LPSC. Figure 1c,d illustrates the stark difference in the tortuosity between the coarse- and fine-LPSC cathode composites structures. In the coarse-LPSC cathode composite, Li ions must navigate a more circuitous route, while the fine-LPSC provides more direct pathways. The reduced tortuosity of the fine-LPSC structure significantly enhances Li ion transportation during (de)lithiation.

EIS measurements were conducted to investigate the Li ion transport kinetics for both cathode composites with the cathode composite/LPSC/Li full cell configuration.[23] Typical EIS plots are shown in Figure 1e, where three semicircles can be identified using an equivalent circuit model, including the bulk resistance of the SSE (R_b), the SEI interface resistance (R_{SEI}), and the charge transfer interface resistance (R_{CT}).[24] The significant change in impedance occurs at R_{ct}, where the resistance of the fine-LPSC cathode composite decreases from 17.3 Ω in the coarse-LPSC cathode composite to 9.9 Ω. The corresponding distribution of relaxation time (DRT) curves

https://doi.org/10.1021/acsenergylett.4c03256
ACS Energy Lett. 2025, 10, 966−974

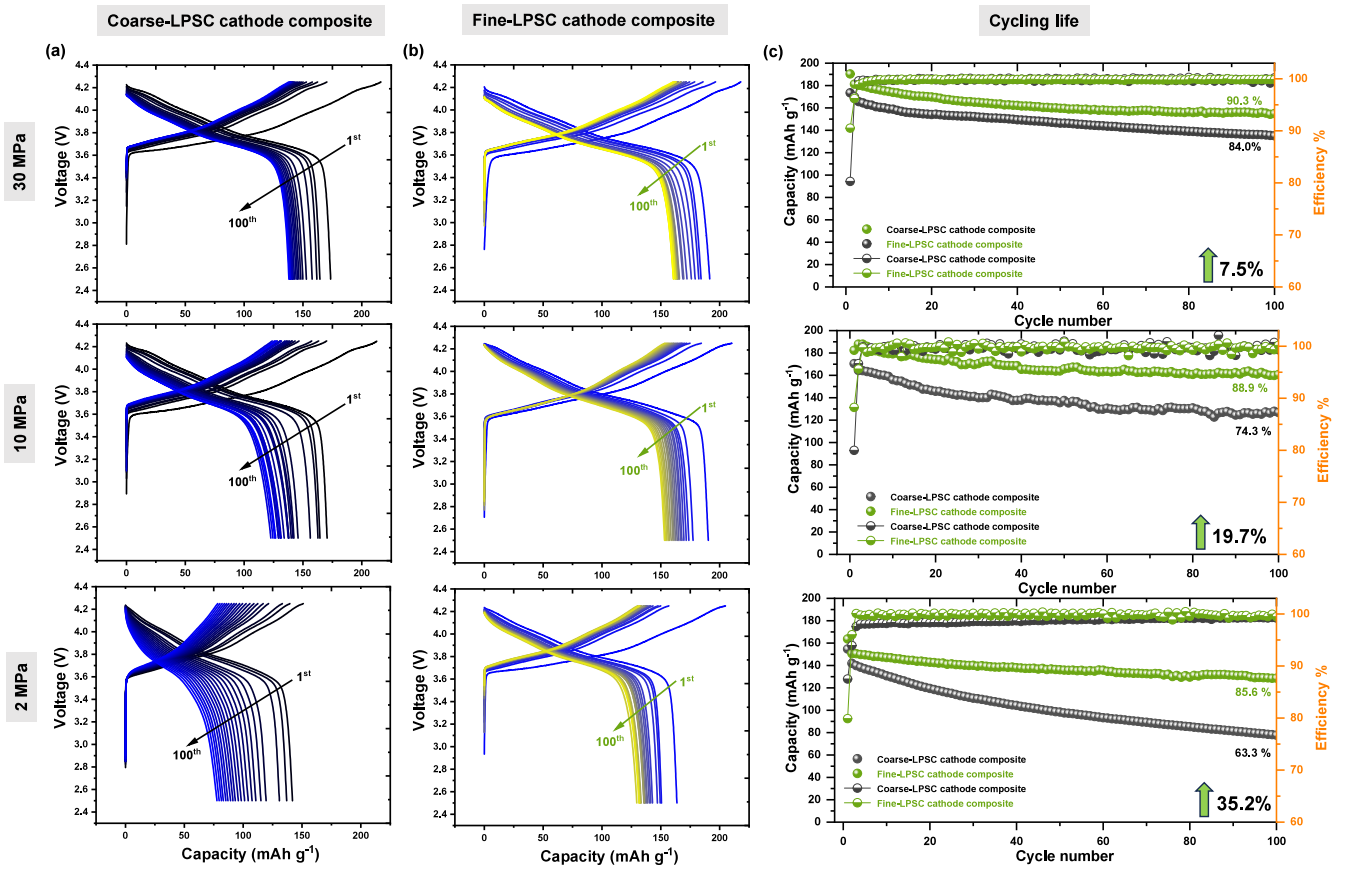

Figure 2. Electrochemical performance of ASSBs employing the coarse-LPSC cathode composite and fine-LPSC cathode composite at 0.1 C, 30 °C, and different pressures. Charge−discharge voltage profiles for the coarse-LPSC cathode composite (a) and the fine-LPSC cathode composite (b) under 30, 10, and 2 MPa. (c) Cycling performance of the coarse-LPSC cathode composite and fine-LPSC cathode composite under 30, 10, and 2 MPa.

are shown in Figure 1f. Figure S16 provides a detailed analysis of the seven peaks, labeled P1−P7, with a focus on the changes observed in peaks P1 to P4. Notably, the grain boundary resistance at P1 decreases, while its time constant increases from 0.5 to 1.4 μs for the fine-LPSC cathode composite. Since the time constant (τ) is the product of resistance (R) and capacitance (C), the increase in time constant indicates a rise in the capacitance at the grain boundaries, which becomes the dominant factor in the system. Typically, capacitance is positively correlated with the electrochemical surface area.[24] Since the chemical composition remains unchanged, the observed enhancement in capacitance is attributed to the increased interfacial area, consistent with the reduction in the particle size of the fine-LPSC cathode composite. Moreover, the peak P4 can be directly identified associated with the charge transfer process of the cathode interface from Figure S16, exhibiting a reduction in the fine-LPSC cathode composite, similar to the behavior observed in Figure 1e. This demonstrates that the fine-LPSC electrolyte effectively enhances Li ion transport within the cathode composite and promotes improved charge transfer kinetics.[25]

The advantages of the fine-LPSC cathode composite can thus be summarized as follows: (1) the fine-LPSC electrolyte is uniformly distributed around the NCM811 particles in the cathode composite, and (2) it creates continuous diffusion pathways, ensuring sufficient ionic percolation for Li ion transport. These characteristics enable the fine-LPSC electrolyte to enhance direct physical contact between NCM811 and the SSE, thereby facilitating more efficient Li ion transport and percolation.

The electrochemical performance of the fine-LPSC cathode composite is compared with that of the coarse-LPSC cathode composite through capacity, cycling stability, and rate capability tests in ASSBs with NCM811 and a lithium metal anode. As shown in Figures 2a,b and S17, the fine-LPSC cathode composite exhibits higher capacity than the coarse-LPSC cathode composite in the first cycle under all pressure conditions. Specifically, the fine-LPSC cathode composite delivers 18, 20, and 22 mAh g^{-1} higher capacity than the coarse-LPSC cathode composite at 30, 10, and 2 MPa, respectively. These results correlate well with predictions from the utilization simulation, where a higher utilization corresponds to a higher capacity. The coarse-LPSC cathode composite achieves approximately 85% of the capacity of the fine-LPSC cathode composite. The slight discrepancy between the experimental results and simulations may indicate that further refinement of particle overlap is needed for the specific C-rate used.

As cycling progressed, the coarse-LPSC cathode composite showed significant capacity degradation, with 84.0%, 74.3%, and 63.3% capacity retention after 100 cycles at 30, 10, and 2 MPa, respectively (Figure 2c). In contrast, the fine-LPSC cathode composite demonstrated superior cycling stability, retaining 90.3% and 88.9% capacity at 30 and 10 MPa, respectively, representing improvements of 7.5% and 19.7%. Notably, at 2 MPa, the fine-LPSC cathode composite retained

https://doi.org/10.1021/acsenergylett.4c03256
ACS Energy Lett. 2025, 10, 966−974

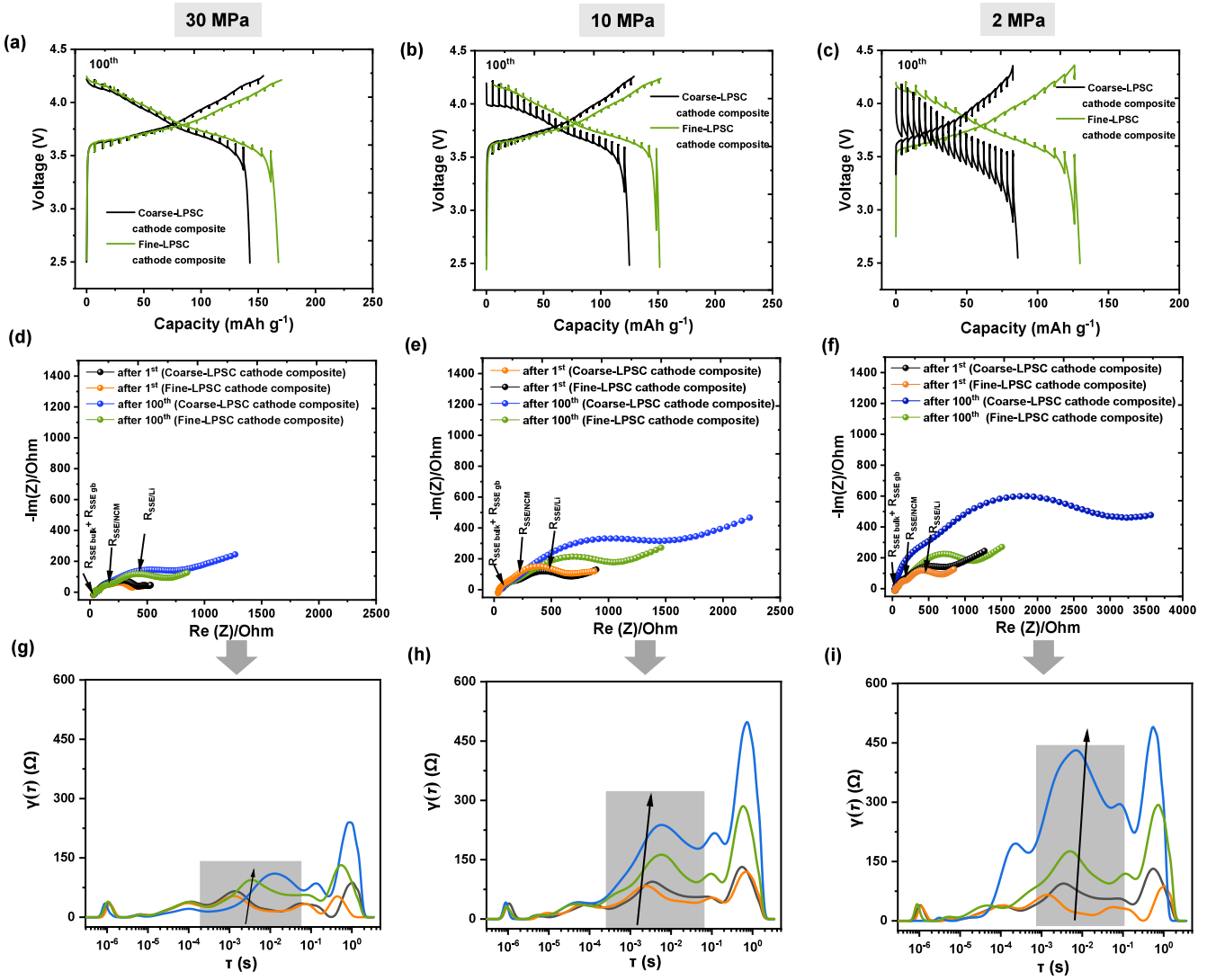

Figure 3. GITT curves of the coarse-LPSC cathode composite and fine-LPSC cathode composite at 30 (a), 10 (b), and 2 MPa (c) after 100 cycles. Nyquist and corresponding DRT plots for the coarse-LPSC cathode composite and fine-LPSC cathode composite at 30 MPa (d, g), 10 MPa (e, h), and 2 MPa (f, i) after 1 and 100 cycles.

85.6% capacity, a significant improvement of 35.2%. The rate capability was also evaluated by cycling the cells at various current densities (0.1, 0.2, 0.3, and 0.5 C) for five cycles, as shown in Figure S18. The fine-LPSC cathode composite exhibited 40% and 50% higher capacity than the coarse-LPSC cathode composite at 0.3 and 0.5 C, respectively. These results demonstrate that the fine-LPSC cathode composite significantly enhances the long-term cycling stability and rate performance of NCM811 in ASSBs, particularly at lower stack pressures (2 MPa).

Galvanostatic intermittent titration technique (GITT) measurements were conducted on both cathode composites after 100 cycles to assess the polarization behavior. The results, shown in Figure 3a–c, reveal that the fine-LPSC cathode composite exhibits lower polarization compared to the coarse-LPSC cathode composite at 30 and 10 MPa, with the difference being especially pronounced at 2 MPa. Polarization is indicative of incomplete solid–solid contacts between the SSE and NCM811 particles, which may be due to uneven contact or microvoids and cracks within the internal regions of the NCM811 particles—an issue we will address later. This finding supports the observation that Li ion transport percolation is more effective in the fine-LPSC cathode composite than in the coarse-LPSC cathode composite after long-term cycling at 2 MPa.

EIS measurements were performed to obtain the Nyquist plots for both cathode composites after 1 and 100 cycles at 30, 10, and 2 MPa, respectively (Figure 3d–f). These plots show the bulk resistance of the SSE (the grain boundary resistance, R_{SSE} bulk + R_{SSE} gb), the interface resistance between the SSE and cathode (R_{SSE}/NCM), as well as the interface resistance between the SSE and the anode (R_{SSE}/anode).[26] The calculated resistance values for all samples are presented by fitting the EIS data in Figure S19. At 30 MPa, the R_{SSE}/NCM resistance values after 100 cycles for both composites show a significant increase compared to their initial states, indicating the increase of the charge transfer resistance (R_{ct}) and the CEI resistance (R_{CEI}), which can be attributed to the deterioration of the bulk NCM811 structure and interfacial solid–solid contact during cycling. Notably, as the pressure decreases, the coarse-LPSC cathode composite exhibits much higher R_{SSE}/NCM resistance than the fine-LPSC cathode composite,

https://doi.org/10.1021/acsenergylett.4c03256
ACS Energy Lett. 2025, 10, 966–974

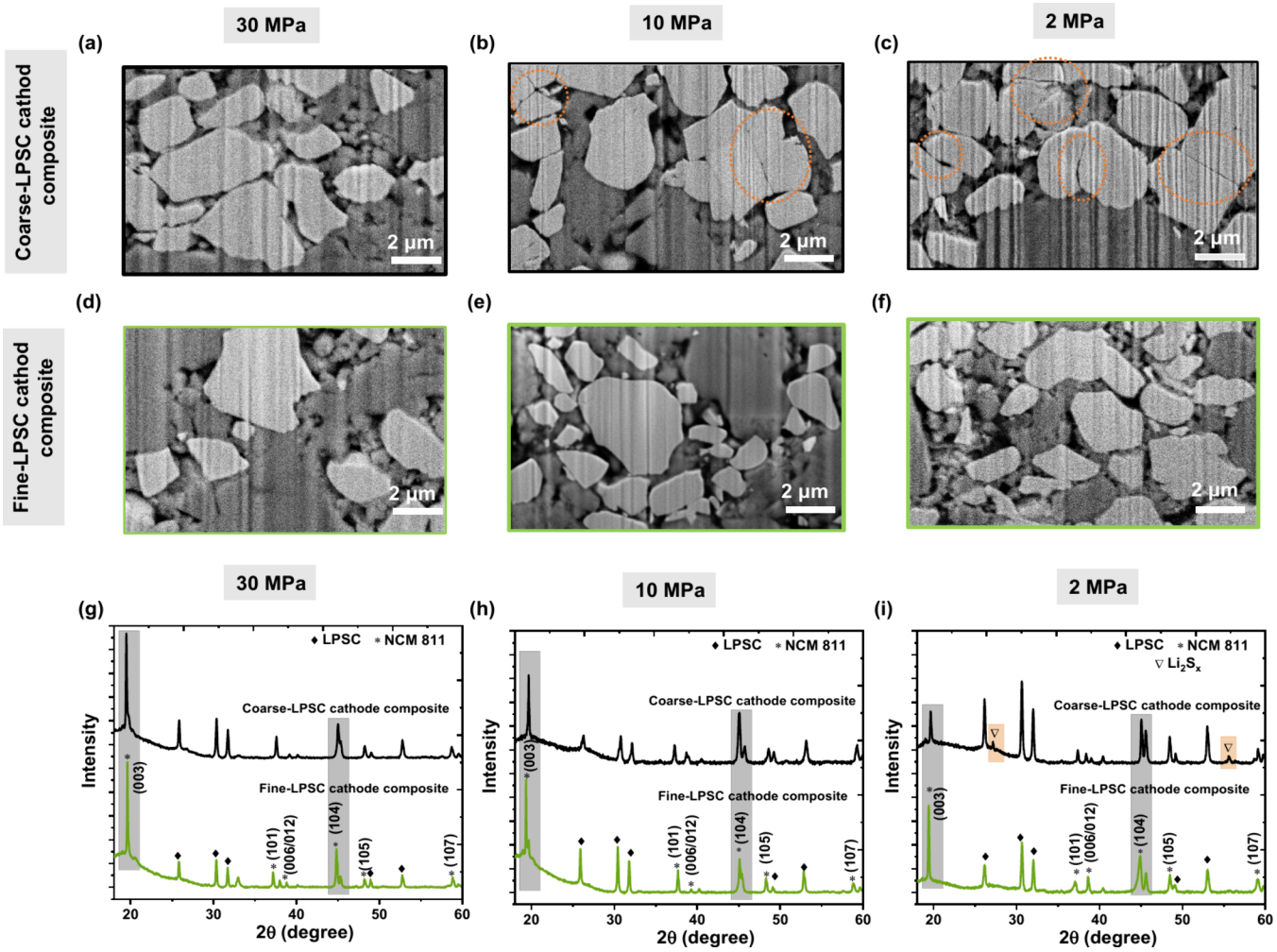

Figure 4. Structural stability. (a–f) FIB-SEM cross-sectional image of the coarse-LPSC cathode composite and fine-LPSC cathode composite after 100 cycles at 30, 10, and 2 MPa. (g–i) XRD patterns of the coarse-LPSC cathode composite and fine-LPSC cathode composite after 100 cycles at 30, 10, and 2 MPa.

implying severe decay of the crystal structure and interface. Specifically, at 2 MPa, the resistance of the coarse-LPSC cathode composite increases by 545 Ω, while the fine-LPSC cathode composite sees an increase of only 34 Ω. We attribute this to a more uniform stress exerted by the NCM811/LPSC composite during cycling. The effect of pressure in mitigating degradation is thus more pronounced with coarse-LPSC composites. Finally, we note that the Li/SSE interface also deteriorates with cycling at all pressures. However, the fine-LPSC composite cells experience a smaller increase in the Li/SSE impedance. Figure 3g–i shows the corresponding DRT plots for both cathode composites after 1 and 100 cycles at 30, 10, and 2 MPa. Relaxation times of 10^{-4}–10^{-1} s are associated with the impedance of the charge transfer process in the cathode and anode sides (gray area).[27] The area of the DRT peak can indicate relative polarization resistance and reflect variations in the rate of the electrode reactions.[28] It is observed that the area of the coarse-LPSC cathode composite increases by 8% and 26% at 30 and 10 MPa, respectively, after 100 cycles, compared to the fine-LPSC cathode composite. However, at 2 MPa, the coarse-LPSC cathode composite shows a marked increase of 115% relative to that of the fine-LPSC cathode composite, suggesting much slower charge-transfer kinetics.

To investigate the decomposition of the cathode composites after long-term cycling, X-ray photoelectron spectroscopy (XPS) analysis was performed, as shown in Figure S20. The S 2p spectra indicate that as the stack pressure decreases from 30 to 2 MPa, the decomposition products, including P_2S_x (polysulfides) and Li_2S_x, increase in both cathode composites. The signal at 161.7 eV, which corresponds to the SSE component PS_4^{2-}, gradually diminishes, further highlighting the changes occurring within the cathode composites as a result of prolonged cycling. Meanwhile, it is evident that the parasitic side reactions at the interface are much less severe for the fine-LPSC cathode composite compared to the coarse-LPSC cathode composite during extended cycling. This observation can be attributed to the effect of the current and potential distribution in the cathode composite. When the structure is nonuniform with poor NCM811 and LPSC contact, local hot spots with high current densities and polarizations can accelerate the degradation of the SSE. In contrast, intimate contacts in the fine-LPSC composite will increase the SSE/NCM811 contact area but with much less possibility of enhanced local degradation.

These results suggest that the structure of the cathode composite has a minimal impact on Li ion transport at high stack pressures. However, as the pressure decreases, the

https://doi.org/10.1021/acsenergylett.4c03256
ACS Energy Lett. 2025, 10, 966–974

structure of the composite electrode becomes increasingly important. The fine-LPSC cathode composite significantly improves the Li ion transport stability at low pressure, leading to enhanced cycling performance over time.

The structural stability of both cathode composites after cycling was investigated by using cross-sectional SEM and XRD analysis. Upon comparing the cross-sectional morphology of the two cathode composites after long-term cycling, the coarse-LPSC cathode composite shows the formation of microcracks on the NCM811 particles at 10 MPa compared to that at 30 MPa (Figure 4a-b), with more pronounced cracking observed at 2 MPa (Figure 4c). These cracks likely result from structural changes in the NCM811 particles. Inhomogeneous current flow to the active material due to the poor contact with SSE leads to local overcharge and overdischarge, which are known to cause Li^+/Ni^{2+} mixing, lattice distortions, and particle strain, which can eventually result in crack formation.[29] As expected, the fine-LPSC cathode composite exhibits significantly fewer cracks (Figure 4d−f), maintaining better Li ion transport stability at the interface.

XRD analysis (Figure 4g−i) shows that the diffraction patterns for both cathode composites align with the layered hexagonal α-$NaFeO_2$ crystal structure ($R\bar{3}m$ space group) for NCM811 particles and the cubic argyrodite-type structure ($F\bar{4}3m$ space group) for LPSC particles. However, the coarse-LPSC cathode composite displays additional impurity peaks of polysulfide (Li_2S_x),[30] under 2 MPa, suggesting the slight decomposition of SSE.[31] Additionally, the I(003)/I(104) ratio, which reflects the degree of Li/Ni mixing in the NCM811 material, varied across the samples. A higher ratio indicates less Li/Ni mixing.[32] At 30 MPa (Figure 4g), no significant changes were observed in either cathode. However, at 10 (Figure 4h) and 2 MPa (Figure 4i), the ratios for the coarse-LPSC cathode and fine-LPSC cathode composites are 1.121 and 1.388 at 10 MPa and 1.011 and 1.204 at 2 MPa, respectively. This suggests that the fine-LPSC cathode composite has a lower degree of Li/Ni mixing as a result of more uniform Li ion conduction pathways and more stable crystal structure compared to the coarse-LPSC cathode composite.[33]

High-resolution scanning transmission electron microscopy (STEM) images of the coarse-LPSC cathode composite after 100 cycles at 2 MPa (Figure S21a) reveal the presence of a rock-salt phase ($Fm\bar{3}m$) layer on the outer surface, indicating severe Li/Ni mixing and surface parasitic reactions, which result in undesirable phase transitions. These transitions further exacerbate structural degradation and hinder Li ion diffusion, leading to electrochemical performance degradation. In contrast, no irreversible phase transition was observed in the fine-LPSC cathode composite (Figure S21b), highlighting its greater structural stability and better performance over long-term cycling at a low pressure. Overall, these findings suggest that the fine-LPSC cathode composite exhibits a higher resistance to mechanical degradation and structural instability, which is consistent with its improved cycle retention at 2 MPa.

In summary, we introduce a simple roll-mixing method using a toluene solution to prepare a fine-LPSC SSE, which is then incorporated into the cathode composite. We find that most of these particles are 1−3 μm in size, with others below 1 μm. This size distribution, which is slightly smaller than that of our NCM811 particles, generates a uniform distribution of the SSE on the surface of each NCM811 particle in the cathode composite, facilitating the formation of a homogeneous Liion percolation network and reducing tortuosity for Li ion transport. As a result, the fine-LPSC cathode composite maintains intimate contact between the CAM and SSE, leading to a higher reversible discharge capacity and improved cycling stability—retaining 85.6% capacity after 100 cycles at 2 MPa, compared to just 63.3% for the coarse-LPSC cathode composite. Through comprehensive electrochemical testing and multiscale characterizations, we demonstrate that the quality of the cathode composite microstructure plays a critical role in achieving high electrochemical performance, particularly at low pressures (e.g., 2 MPa). For the coarse-LPSC cathode composite, the electrochemically inactive interface leads to significant resistance and chemomechanical degradation after extended cycling. In contrast, the fine-LPSC cathode composite effectively suppresses increases in charge transfer resistance and mechanical degradation, ensuring better structural stability over time. Our findings provide valuable insights into the design of cathode composite architectures optimized for low-pressure cycling, offering a promising approach to accelerate the commercialization of ASSBs.

■ ASSOCIATED CONTENT

Supporting Information

The Supporting Information is available free of charge at https://pubs.acs.org/doi/10.1021/acsenergylett.4c03256.

Experimental details for material preparation, material characterization, simulation method, cell assembly, and electrochemical characterization procedures; schematics of synthesis process; morphology, particle size distribution, crystal structure, conductivity, and thermal analysis of fine and coarse electrolyte particles; surface area, density, and porosity analyses of the pellets; imaging and elemental mapping of cathode composites; microstructural modeling of cathode composites; impedance analysis; post-mortem analysis; table of impedance relaxation analysis (PDF)

■ AUTHOR INFORMATION

Corresponding Authors

Hyunsun Alicia Kim − *Aiiso Yufeng Li Family Department of Chemical and Nano Engineering, University of California, San Diego, La Jolla, California 92093, United States*; Email: hak113@ucsd.edu

Ping Liu − *Aiiso Yufeng Li Family Department of Chemical and Nano Engineering, University of California, San Diego, La Jolla, California 92093, United States; Program of Material Science and Program of Chemical Engineering, University of California San Diego, La Jolla, California 92093, United States*; orcid.org/0000-0002-1488-1668; Email: piliu@ucsd.edu

Authors

Ke Zhou − *Aiiso Yufeng Li Family Department of Chemical and Nano Engineering, University of California, San Diego, La Jolla, California 92093, United States*

Sijian Lu − *Aiiso Yufeng Li Family Department of Chemical and Nano Engineering, University of California, San Diego, La Jolla, California 92093, United States*

Charles Mish − *Aiiso Yufeng Li Family Department of Chemical and Nano Engineering, University of California, San Diego, La Jolla, California 92093, United States*

https://doi.org/10.1021/acsenergylett.4c03256
ACS Energy Lett. 2025, 10, 966−974

Yu-Ting Chen − *Aiiso Yufeng Li Family Department of Chemical and Nano Engineering, University of California, San Diego, La Jolla, California 92093, United States*
Shijie Feng − *Aiiso Yufeng Li Family Department of Chemical and Nano Engineering, University of California, San Diego, La Jolla, California 92093, United States;* orcid.org/0000-0001-5797-8542
Jiyoung Kim − *LG Energy Solution, Ltd., Gangseo-gu, Seoul 07796, Republic of South Korea*
Min-Sang Song − *LG Energy Solution, Ltd., Gangseo-gu, Seoul 07796, Republic of South Korea*

Complete contact information is available at: https://pubs.acs.org/10.1021/acsenergylett.4c03256

Notes

The authors declare no competing financial interest.

■ ACKNOWLEDGMENTS

This work was supported by LG Energy Solution−U.C. San Diego Frontier Research Laboratory (FRL) via the Open Innovation program. We would like to thank Wenxuan Hu from Xiamen University for his help with the EIS analysis.

■ REFERENCES

(1) Wan, H.; Xu, J.; Wang, C. Designing electrolytes and interphases for high-energy lithium batteries. *Nat. Rev. Chem.* **2024**, *8* (1), 30−44. From NLM PubMed-not-MEDLINE
(2) Janek, J.; Zeier, W. G. Challenges in speeding up solid-state battery development. *Nat.Energy* **2023**, *8* (3), 230−240.
(3) Zeng, Z.; Cheng, J.; Li, Y.; Zhang, H.; Li, D.; Liu, H.; Ji, F.; Sun, Q.; Ci, L. Composite cathode for all-solid-state lithium batteries: Progress and perspective. *Mater.Today Phys.* **2023**, *32*, 101009.
(4) Minnmann, P.; Strauss, F.; Bielefeld, A.; Ruess, R.; Adelhelm, P.; Burkhardt, S.; Dreyer, S. L.; Trevisanello, E.; Ehrenberg, H.; Brezesinski, T.; et al. Designing cathodes and cathode active materials for solid-state batteries. *Adv. Energy Mater.* **2022**, *12*, 2201425.
(5) Chen, R.; Li, Q.; Yu, X.; Chen, L.; Li, H. Approaching practically accessible solid-state batteries: stability issues related to solid electrolytes and interfaces. *Chem. Rev.* **2020**, *120* (14), 6820−6877. From NLM PubMed-not-MEDLINE
(6) Koerver, R.; Zhang, W.; de Biasi, L.; Schweidler, S.; Kondrakov, A. O.; Kolling, S.; Brezesinski, T.; Hartmann, P.; Zeier, W. G.; Janek, J. Chemo-mechanical expansion of lithium electrode materials − on the route to mechanically optimized all-solid-state batteries. *Energy Environ. Sci.* **2018**, *11* (8), 2142−2158.
(7) Zheng, Y.; Yao, Y.; Ou, J.; Li, M.; Luo, D.; Dou, H.; Li, Z.; Amine, K.; Yu, A.; Chen, Z. A review of composite solid-state electrolytes for lithium batteries: fundamentals, key materials and advanced structures. *Chem. Soc. Rev.* **2020**, *49* (23), 8790−8839.
(8) Zaman, W.; Hatzell, K. B. Processing and manufacturing of next generation lithium-based all solid-state batteries. *Curr. Opin. Solid State Mater. Sci.* **2022**, *26* (4), 101003.
(9) Kalnaus, S.; Dudney, N. J.; Westover, A. S.; Herbert, E.; Hackney, S. Solid-state batteries: The critical role of mechanics. *Science* **2023**, *381* (6664), No. eabg5998. From NLM PubMed-not-MEDLINE
(10) Pang, Y.; Pan, J.; Yang, J.; Zheng, S.; Wang, C. Electrolyte/electrode interfaces in all-solid-state lithium batteries: a review. *Electrochem. Energy Rev.* **2021**, *4* (2), 169−193.
(11) Xu, H.; Yang, S.; Li, B. Pressure effects and countermeasures in solid-state batteries: a comprehensive review. *Adv. Energy Mater.* **2024**, *14* (16), No. 2303539.
(12) Sakka, Y.; Yamashige, H.; Watanabe, A.; Takeuchi, A.; Uesugi, M.; Uesugi, K.; Orikasa, Y. Pressure dependence on the three-dimensional structure of a composite electrode in an all-solid-state battery. *J. Mater. Chem. A* **2022**, *10* (31), 16602−16609.
(13) Schlautmann, E.; Weiß, A.; Maus, O.; Ketter, L.; Rana, M.; Puls, S.; Nickel, V.; Gabbey, C.; Hartnig, C.; Bielefeld, A.; et al. Impact of the solid electrolyte particle size distribution in sulfide-based solid-state battery composites. *Adv. Energy Mater.* **2023**, *13* (41), 2302309−2302318.
(14) Shi, T.; Tu, Q.; Tian, Y.; Xiao, Y.; Miara, L. J.; Kononova, O.; Ceder, G. High active material loading in all-solid-state battery electrode via particle size optimization. *Adv. Energy Mater.* **2020**, *10* (1), 1902881−1902890.
(15) Strauss, F.; Bartsch, T.; de Biasi, L.; Kim, A. Y.; Janek, J.; Hartmann, P.; Brezesinski, T. Impact of cathode material particles size on the capacity of bulk-type all-solid-state batteries. *ACS Energy Lett.* **2018**, *3* (4), 992−996.
(16) Wang, Y.; Li, X. Fast kinetics design for solid-state battery device. *Adv. Mater.* **2024**, *36* (15), 2309306−2309315. From NLM PubMed-not-MEDLINE
(17) Kim, J. T.; Shin, H.-J.; Kim, A. Y.; Oh, H.; Kim, H.; Yu, S.; Kim, H.; Chung, K. Y.; Kim, J.; Sun, Y.-K.; et al. An argyrodite sulfide coated NCM cathode for improved interfacial contact in normal-pressure operational all-solid-state batteries. *J. Mater. Chem. A* **2023**, *11* (38), 20549−20558.
(18) Oh, J.; Choi, S. H.; Kim, J. Y.; Lee, J.; Lee, T.; Lee, N.; Lee, T.; Sohn, Y.; Chung, W. J.; Bae, K. Y.; et al. Anode-less all-solid-state batteries operating at room temperature and low pressure. *Adv. Energy Mater.* **2023**, *13* (38), 2301508−2301517.
(19) Yao, X.; Liu, D.; Wang, C.; Long, P.; Peng, G.; Hu, Y. S.; Li, H.; Chen, L.; Xu, X. High-energy all-solid-state lithium batteries with ultralong cycle Life. *Nano Lett.* **2016**, *16* (11), 7148−7154. From NLM PubMed-not-MEDLINE
(20) Jang, G.-J.; Rajagopal, R.; Kang, S.; Ryu, K.-S. Preparation of argyrodite $Li_{6-2x}Zn_xPS_{5-x}O_xCl$ with improved electrochemical performance and air stability for all-solid-state batteries. *J. Alloys Compd.* **2023**, *957* (25), 170273−170283.
(21) Plimpton, S. *Pair style granular interactions in LAMMPS*. Sandia National Laboratories, 2024.
(22) Tjaden, B.; Cooper, S. J.; Brett, D. J. L.; Kramer, D.; Shearing, P. R. On the origin and application of the Bruggeman correlation for analysing transport phenomena in electrochemical systems. *Curr.Opin. Chem. Eng.* **2016**, *12*, 44−51.
(23) Orue Mendizabal, A.; Cheddadi, M.; Tron, A.; Beutl, A.; Lopez-Aranguren, P. Understanding interfaces at the positive and negative electrodes on sulfide-based solid-state batteries. *ACS Appl.Energy Mater.* **2023**, *6* (21), 11030−11042. From NLM PubMed-not-MEDLINE
(24) Vadhva, P.; Hu, J.; Johnson, M. J.; Stocker, R.; Braglia, M.; Brett, D. J. L.; Rettie, A. J. E. Electrochemical impedance spectroscopy for all-solid-state batteries: theory, methods and future outlook. *ChemElectroChem.* **2021**, *8* (11), 1930−1947.
(25) Gantenbein, S.; Weiss, M.; Ivers-Tiffée, E. Impedance based time-domain modeling of lithium-ion batteries: Part I. *J. Power Sources* **2018**, *379* (1), 317−327.
(26) Gaberscek, M. Understanding Li-based battery materials via electrochemical impedance spectroscopy. *Nat. Commun.* **2021**, *12* (1), 6513. From NLM PubMed-not-MEDLINE
(27) Lu, Y.; Zhao, C.-Z.; Huang, J.-Q.; Zhang, Q. The timescale identification decoupling complicated kinetic processes in lithium batteries. *Joule* **2022**, *6* (6), 1172−1198.
(28) Cai, X.; Zhang, C.; Ruan, H.; Chen, Z.; Zhang, L.; Sauer, D. U.; Li, W. Cross-scale decoupling kinetic processes in lithium-ion batteries using the multi-dimensional distribution of relaxation time. *Adv. Sci.* **2024**, *11* (44), 2406934−2406952. From NLM PubMed-not-MEDLINE
(29) Fan, X.; Hu, G.; Zhang, B.; Ou, X.; Zhang, J.; Zhao, W.; Jia, H.; Zou, L.; Li, P.; Yang, Y. Crack-free single-crystalline Ni-rich layered NCM cathode enable superior cycling performance of lithium-ion batteries. *Nano Energy* **2020**, *70*, 104450−102261.
(30) Xu, R.; Belharouak, I.; Zhang, X.; Chamoun, R.; Yu, C.; Ren, Y.; Nie, A.; Shahbazian-Yassar, R.; Lu, J.; Li, J. C.; et al. Insight into

sulfur reactions in Li-S batteries. *ACS Appl. Mater. Interfaces* **2014**, *6* (24), 21938−21945. From NLM PubMed-not-MEDLINE

(31) Wu, Y.; Zhou, K.; Ren, F.; Ha, Y.; Liang, Z.; Zheng, X.; Wang, Z.; Yang, W.; Zhang, M.; Luo, M.; et al. Highly reversible Li2RuO3 cathodes in sulfide-based all solid-state lithium batteries. *Energy Environ. Sci.* **2022**, *15* (8), 3470−3482.

(32) Liu, H.; Yang, R.; Yang, W.; Bai, C.; Li, Y.-C.; Wang, G.; Liu, Y.; Xiang, W.; Wu, Z.; Guo, X. Suppressing capacity fading and voltage decay of Ni-rich cathode material by dual-ion doping for lithium-ion batteries. *J. Mater. Sci.* **2021**, *56* (3), 2347−2359.

(33) Wang, B.; Zhang, F.; Zhou, X.; Wang, P.; Wang, J.; Ding, H.; Dong, H.; Liang, W.; Zhang, N.; Li, S. Which of the nickel-rich NCM and NCA is structurally superior as a cathode material for lithium-ion batteries? *J.Mater. Chem. A* **2021**, *9* (23), 13540−13551.

https://doi.org/10.1021/acsenergylett.4c03256
ACS Energy Lett. 2025, 10, 966−974